arXiv:1403.4989v1 [cond-mat.mtrl-sci] 19 Mar 2014

Longitudinal spin-Seebeck effect and huge growth of thermoelectric parameters at band edges in H- and F-doped graphene, free-standing and deposited on $4H$-SiC(0001) C-face

Małgorzata Wierzbowska*
Institute of Theoretical Physics, Faculty of Physics, University of Warsaw, ul. Hoża 69, 00-681 Warszawa, Poland

Adam Dominiak†
Institute of Heat Engineering, Faculty of Power and Aeronautical Engineering, Warsaw University of Technology, ul. Nowowiejska 21/25, 00-665 Warszawa, Poland

(Dated: March 21, 2014)

Graphene halfly doped with H or F possesses local magnetization at the undoped C sites. Thus the Seebeck coefficient is different for each spin channel and its sign also changes depending on the spin polarization. Deposition of doped graphene on the C-face $4H$-SiC(0001) with two buffer layers substantially varies the electronic and thermoelectric properties. These properties are efficiently calculated from the semiclassical Boltzmann equations, using the maximally-localized Wannier-functions interpolation of the band structures obtained with the density-functional theory. Our results indicate large growth of the thermopower and the ZT efficiency at the band edges. We show in the model discussion that this phenomenon is more general and applies also to other systems than graphene. It gives prospect for developing new spintronic devices working in the band-edge regime.

PACS numbers: 81.05.ue, 73.22.Pr, 72.80.Vp, 65.80.Ck

1. Introduction

The direct conversion of heat into electrical energy is an intensively studied field for last half century. The crucial issue in this research is finding new materials with specific thermal and electric properties. The semiconductor materials development extends applications concerning thermoelectric effects like Seebeck and Peltier, which are the basic phenomena among other non-equilibrium thermoelectric effects. Seebeck effect is the electric voltage generation in a conductor under a temperature gradient, and it is used in the heat sink applications. With the inverse effect, namely Peltier, an active cooling can be received. Recent studies on spintronics and spin-caloritronics [1] revealed a spin analogue of the Seebeck effect, which can occur in magnets, also insulating [2, 3]. Spin-Seebeck effect can be longitudinal e.g. caused by magnon-induced spin current injected from a ferromagnet [4, 5], or transverse e.g. from the substrate [6, 7]. Spin-dependent Peltier effect has been also observed [8].

The dimensionless figure of merit $ZT = \sigma S^2 T/\kappa$ gives a measure of the system efficiency in the thermoelectric effects. The Seebeck coefficient (S) describes the electric voltage generation under the temperature gradient stimulus through the sample with no electrical current. It is an intrinsic parameter of each material and depends on temperature (T). Higher electrical conductivity (σ), lower thermal conductivity (κ), and higher Seebeck coefficient are necessary for better and more effective thermoelectric materials. Finding new materials with higher ZT factor is difficult, because the thermal conductivity is strongly positively related with the electrical conductivity, due to the fact that both are depended on crystal and electronic structures and carrier concentration. These physical properties stay in conflict to each other. The ZT factor easily allows to compare the performance of thermoelectric devices based on particular materials. For the thermoelectric devices which could be competitive with the mechanical devices (power generation or cooling), the ZT should be about 3. The value of ZT equal to 1 was reached in 1990s, the value of 2 is now technically available but at high temperatures only [9, 10].

About two-thirds of all energy used worldwide is dissipated as heat and the demand for an alternative technology to reduce fossil fuels use, along with their environmental impact, leads to important regiments of research fields including that of direct thermal-electrical energy conversion via thermoelectricity. Seebeck and Peltier effects applied within proper materials can solve part of the problems faced ahead sustainable growth. As the semiconductor materials are promising for waste-heat recovery, the graphene has been also studied [11]. Gas flow sensor with the use of Seebeck effect and its correlation with Bernoulli law was presented for single layer graphene [12] and multilayer graphene [13]. These results demonstrate that graphene has great potential for flow sensors and energy conversion devices. For the graphene nanoribbons, the thermoelectric power including the Nernst and Seebeck effects were studied as well, using the nonequilibrium Greens function approach [14] and by molecular dynmics methods [15, 16]. The calcula-

*Electronic address: malgorzata.wierzbowska@fuw.edu.pl
†Electronic address: adam.dominiak@itc.pw.edu.pl

tions of graphene behavior in the magnetic field and the related anomalous thermoelectric effects were reported in [17]. Semiclassical approach for the electronic-density dependence of the dc-conductivity, the optical conductivity, the thermal conductivity, the thermopower, and the classical Hall effect in graphene has been proposed in [18]. The first-principles band-structure calculations were also performed for the spin-caloritronics in the zigzag graphene nanoribbons [19]. Nanocarbon related systems were investigated as thermoelectric-parameter enhanced materials [20].

The effect of the carbon defect in the graphene structure - hydrogen doping and/or carbon vacancy - on magnetism has been proposed in [21]. Recent theoretical studies of halfly doped graphene with hydrogen and also fluorine concluded that the magnetism in this system, as it is usual for the triangular lattice, is probably frustrated and the ferromagnetic state has a bit higher energy [22]. Nevertheless, the local magnetic domains usually form in such systems. It will be interesting to investigate the magnetic states in H- and F-adsorbed graphene at various doping patterns, e.g. rectangular or linear or random. Spin-polarization in graphene can be also obtained by random substitutional doping with B or N, but only sites belonging to one sublattice [23].

In this work, we focus on the ferromagnetic state of halfly doped graphene, free-standing and deposited on the C-face 4H-SiC(0001) substrate with two buffer layers. We calculated the thermoelectric properties by means of the first-priciples methods, and found that the Seebeck effect is spin dependent in both the H- and F-doped systems. We call the effect described here as the longitudinal spin-Seebeck effect, although the carriers were not injected from a ferromagnet to a semiconductor - as it is in most of the investigated longitudinal Seebeck systems. Our effect is purely intrinsic, i.e. it originates from the band structures of two spin-channels in the ferromagnetic graphene. Interestingly, we found large increase of the Seebeck coefficient and also of the ZT efficiency at the band edge. Similar phenomenon has been very recently predicted in the model calculations by Sharapov and Varlamov [24] for gapped graphene. Unusual fact is that, we obtained larger growth of the ZT efficiency not at high temperatures, as common findings in the high-ZT materials, but at lower temperatures.

The paper is organized as follows: we give details of the calculations in section 2, present the results in section 3 - for the free-standing systems in subsection 3.1 and deposited systems in subsection 3.2, analyse the mathematical expressions for the thermoelectric properties using the 1D model band-structures in section 4, and conclude in section 5.

2. Theoretical details

We performed the density-functional theory calculations of the band structures, and applied the Quantum ESPRESSO suit of codes [25] which uses the plane-wave basis set and the pseudopotentials for the core electrons. The exchange-correlation functional was chosen for the gradient corrected Perdew-Wang(91) parametrization. The ultrasoft pseudopotentials were used with the energy cutoffs 20 Ry and 200 Ry for the plane-waves and the density, respectively. The Monkhorst-Pack uniform k-mesh in the Brillouin zone has been set to $40 \times 40 \times 1$ for the free-standing and $10 \times 10 \times 1$ for the deposited graphene sheets. The vacuum separation between the periodic slabs was around 50 Å.

In order to fit the band structure on the very fine k-mesh, i.e. 1600×1600 points in the graphene plane, we employed the wannier90 code [26, 27] which interpolates bands using the maximally-localized Wannier functions [28]. The thermoelectric distribution function and the thermoelectric properties were obtained from the BoltzWann post-processing code [29] with the constant relaxation time set to 10 fs.

The geometric parameters of buckled graphene under H- and F-doping were taken from the work by Rudenko et al. [22]. For the geometry of the doped graphene deposited on the C-face 4H-SiC(0001) surface, we used the $\sqrt{3} \times \sqrt{3}R30^\circ$ supercell to match the graphene

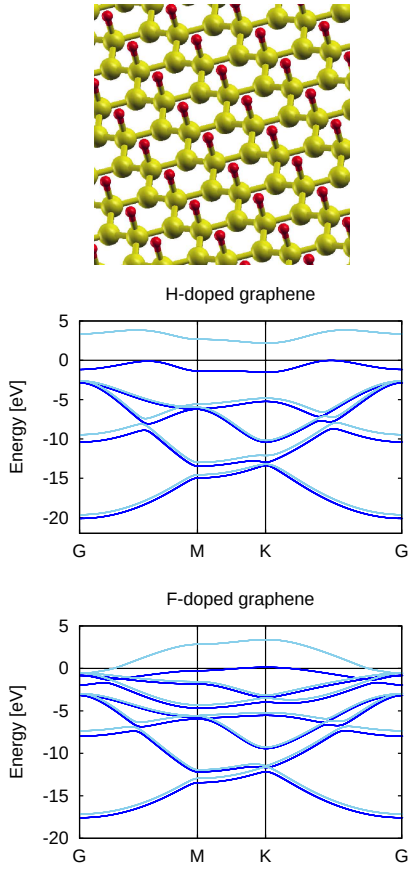

FIG. 1: The atomic structure of graphene halfly doped with H or F, and the band structures of H- and F-doped graphene. The majority spin is printed with the dark-blue color and the minority spin with the light-blue color.

sheets with the substrate. Between the doped graphene and the surface C-atoms, we put two buffer layers in the ABA stacking including the doped top-layer. The interlayer distances were taken from the experimental work by Borysiuk et al. [30].

3. Results

3.1. Free-standing doped graphene monolayer

The adsorption of hydrogen atom on graphene produces the spin-polarization of neighboring carbon atoms [21]. The same occurs for half-doping by hydrogens or fluorines. The magnetic moments per p_z-state of the free C-atom are about 0.76 μ_B and 0.59 μ_B for H- and F-doping, respectively, obtained with the local density approximation in Ref. [22]. Our calculations with the generalized gradient approximation give, as usually for this scheme, higher magnetic moments per C-atom: 1.0 μ_B for H-doping and 0.84 μ_B for F-doping. The top view of the doped graphene layer and the spin-polarized band structures are displayed in Fig. 1. The impurity states in the H-doped case are completely separated on the occupied- and the unoccupied-states sides for the spin-up and spin-down channels, respectively. The experimental confirmation for existence of the separated impurity band in the hydrogenated graphene is given in angle-resolved photoemission spectroscopy (ARPES) studies in Refs. [31, 32]. It is interesting to mention that the local hydrogen doping causes large structural folding of the graphene sheets, which finds various applications [33]. Also the thermal conductivity has been studied for the strained that way graphene sheets [34]. For the F-doped system, the impurity spin-states are separated below and above the Fermi level around the K and M symmetry-points, but close to the middle of the Brillouin zone both spin-states are merged with the valence band. We will show that the above band-structure details have consequences for the thermoelectric properties.

In Fig. 2, we present the density of states (DOS), the Seebeck coefficient and the ZT efficiency for the H-doped graphene, and in Fig. 3 the same properties of the F-doped graphene. In the middle of the impurity bandwidth for both spins and both H- and F-doping, the thermoelectric parameters are very low. But at the separated band edges, the thermopower and the ZT efficiency grows to very high values. This is for both the high- and the low-energy ends of the H-impurity bands, and for the F-impurity bands only at the high-energy band edge. The thermoelectric parameters at the low-energy parts of the F-impurity bands are low, since in that region, the impurity bands touch the valence band manifold. For the spin-down channel of the F-doped graphene, we observe the Seebeck-coefficient and the ZT-efficiency extrema similar to these obtaned for the pure graphene close to the band crossing at the Fermi level near the K-point [35]. Less pronounced features of the same shape in the thermopower curve are visible

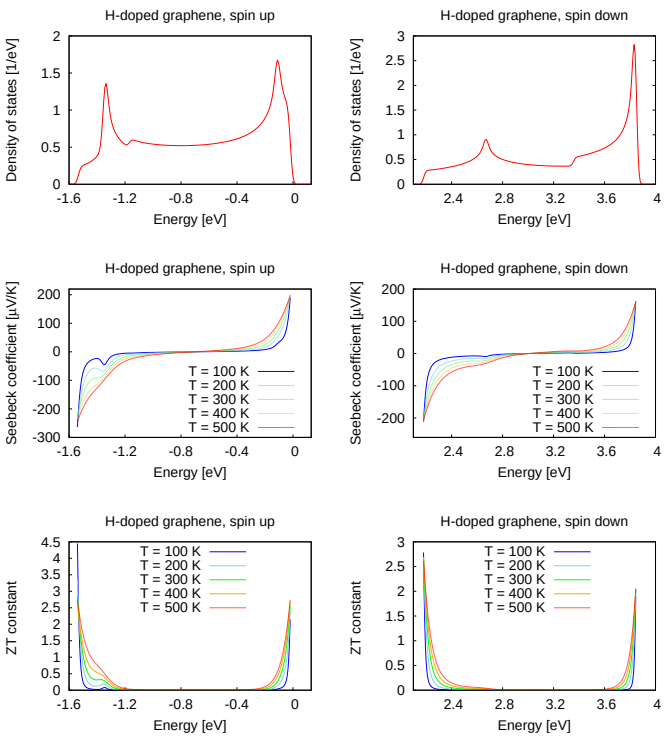

FIG. 2: The density of states, the Seebeck coefficient, and the ZT figure of merit for H-doped graphene.

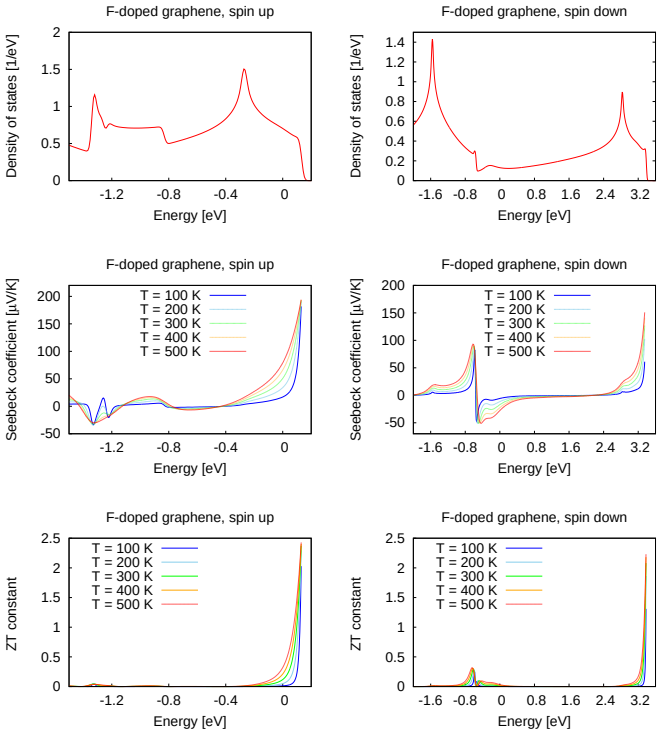

FIG. 3: The density of states, the Seebeck coefficient, and the ZT figure of merit for F-doped graphene.

below -1.2 eV for the spin-up case, and they originate from the band crossings close to the G-point towards the M and K symmetry-points. Since the desired thermoelectric properties occur at the band-edges, we check the shape of the electronic density function. The DOS of all investigated free-standing systems is high or moderate close to the impurity band edges. Thus the enhancement effect of the thermoelectric parameters should be visible in the experiments.

3.2. Doped graphene monolayer deposited on the C-face $4H$-SiC(0001) with two buffer-layers

For the technological reasons, the substrate at which the electronically active layer was deposited or grown is as important as the upper layer itself. The C-face SiC deposited graphene characterizes by very good technological parameters, such as the electron mobility up to 1800 cm^2/Vs, and the defect-free large wafers even 150 mm in diameter can be grown [36]. Moreover, the thermopower parameter of SiC is very good, about -480 μV/K. Therefore SiC can transfer heat from the electronic device [37]. All that made our choice for the substrate for testing the spin-dependent thermoelectric properties of the deposited H- and F-doped graphene.

The atomic structure of doped graphene sheet on top of two buffer layers above the C-face $4H-$SiC(0001) surface is displayed in Fig. 4, together with the band structures of H- and F-doped systems. In the case of hydrogen doping, the majority spin-bands close to the K-point are similar to the bands of bilayer graphene in the AB stacking or graphite [30, 35] - with the difference that here the parabolic bands touch each other below the Fermi level, and the minority spin-bands open the gap close to the K-point. In the case of fluorine doping, the band gap opens at the K-point in both spin channels. For the minority spin, additional bands cross the Fermi level at G and M-point. These details of the band structure rule the thermoelectric properties.

The DOS, the thermopower and the ZT efficiency for the H-doped graphene are presented in Fig. 5, and for the F-doped graphene in Fig. 6. When the gap opens then the thermoelectric parameters jump very high. This situation takes place for the spin-up channel in H-doping and the spin-down channel in F-doping cases. The effect might be more difficult to measure than in the free-standing cases, since the DOS of the deposited doped graphene is lower close to the band edges. The Seebeck coefficient at the temperatures 100, 200, 300, 400 K reaches at maximum values 554, 270, 185, 148 μV/K, respectively, for the H-doped graphene in the spin-down channel, and in the case of the F-doped graphene in the spin-up channel, the thermopower achieves values of 593, 297, 207, 171 μV/K respectively. The ZT efficiency is 15.78, 2.88, 1.19, 0.74 for the H-doped graphene in the spin-down channel at 100, 200, 300, 400 K, respectively, and correspondingly, for the F-doped graphene in the spin-up channel, the ZT figure of merit is 20.10, 3.45, 1.45, 0.95, respectively. It is peculiar and of great application potential, that the thermopower and the ZT figure of merit at the band edges achieve very high values for lower temperatures - in contrast to all other cases known so far in the high-ZT physics.

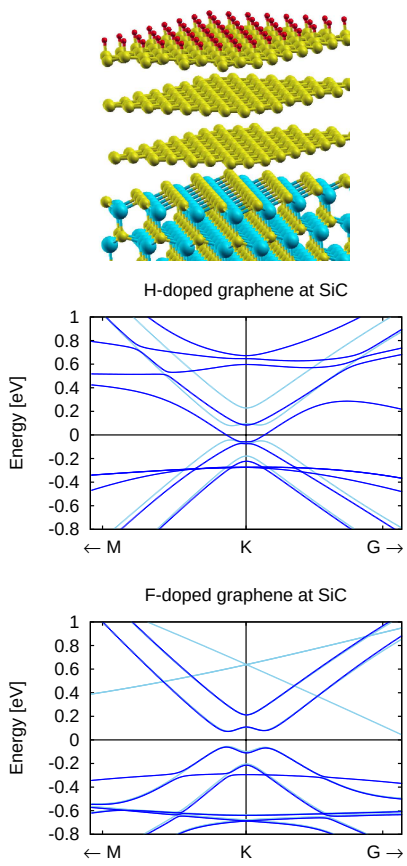

FIG. 4: The atomic structure of graphene doped with H or F and deposited on the C-face SiC(0001) surface with two buffer layers in ABA stacking, and the band structures of H- and F-doped graphene. The majority spin is printed with dark-blue color and the minority spin with light-blue color.

Our finding of the band-edge growth of the Seebeck coefficient and the ZT figure of merit is in agreement with the model predictions by Sharapov and Varlamov [24] for pure gapped graphene. They explained the effect of giant growth of the thermopower at the band gap in graphene assuming the strong dependence of the relaxation time on the energy, i.e. the band details. In this work, we show in the next section that the band-edge growth of the thermopower is caused by vanishing band velocities, independently on the model used for the relaxation time. In both, our work and the model consideretations by Sharapov and Varlamov, the break of the symmetry equivalence between two sublattices in graphene takes place. However, it will be explained below that the effect is more general and applies to all gapped systems independently on their lattices.

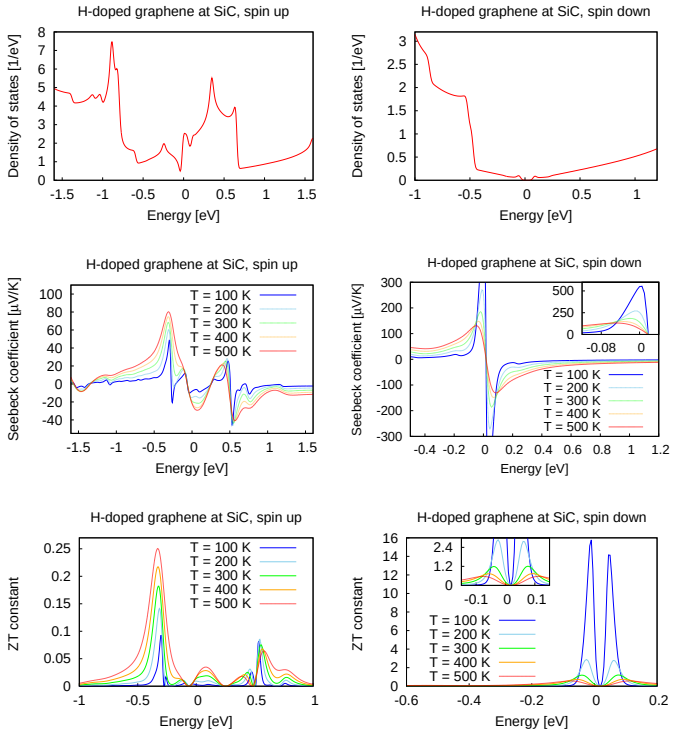

FIG. 5: The density of states, the Seebeck coefficient, and the ZT figure of merit of H-doped graphene deposited on the C-face SiC(0001) surface with two buffer layers.

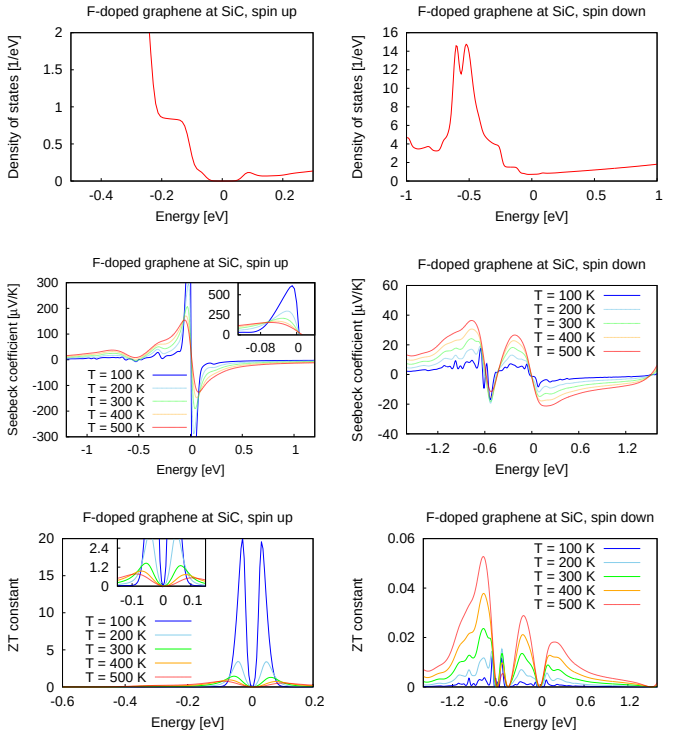

FIG. 6: The density of states, the Seebeck coefficient, and the ZT figure of merit of F-doped graphene deposited on the C-face SiC(0001) surface with two buffer layers.

4. Model studies of a fingerprint of the band-structure features in the thermopower curve

We analyse how the band-structure features such as local extrema and band edges are reflected in the Seebeck-coefficient curve. We begin with the collection of the mathematical expressions.

The transport distribution function (TDF) is a 3D tensor $\Sigma_{ij}(E)$ defined as a function of the energy E as follows:

$$\Sigma_{ij}(E) = \frac{1}{V}\sum_{n,\mathbf{k}} v_i(n,\mathbf{k})v_j(n,\mathbf{k})\,\tau_{n\mathbf{k}}\,\delta(E-E_{n,\mathbf{k}}),$$

$$v_i(n,\mathbf{k}) = \frac{1}{\hbar}\frac{\partial E_{n,\mathbf{k}}}{\partial k_i},$$

where V is the system volume, $v_i(n,\mathbf{k})$ is the band velocity, $E_{n,\mathbf{k}}$ is the band dispersion, and $\tau_{n\mathbf{k}}$ is the relaxation time dependent on the band index n and the reciprocal space $\mathbf{k}$. The TDF enters an expression for the 3D tensor of the Seebeck coefficients S_{ij}, which depends on the chemical potential μ and temperature T, and is defined as:

$$S_{ij}(\mu,T) = \frac{1}{eT}\,K_{ij,1}(\mu,T)\,K^{-1}_{ij,2}(\mu,T),$$

where

$$K_{ij,1}(\mu,T) = \int_{-\infty}^{\infty} dE\,\left(-\frac{\partial f(E,\mu,T)}{\partial E}\right)\,(E-\mu)\,\Sigma_{ij}(E),$$

$$K_{ij,2}(\mu,T) = \int_{-\infty}^{\infty} dE\,\left(-\frac{\partial f(E,\mu,T)}{\partial E}\right)\,\Sigma_{ij}(E).$$

In the above formulae, the function $f(E,\mu,T)$ is the Fermi-Dirac distribution and e is the electron charge.

The system dimension is not crucial for the analysis, therefore for simplicity, we model the bands in 1D and skip the indeeces ij. In Fig. 7, we propose three band structures: 1) isolated symmetric band, 2) isolated asymmetric band, 3) two bands of the previous models together, which partially overlap in the energetic range. The constant relaxation time τ is asumed. We plot also the band velocities and the kernels entering the expression for the thermopower. From the formula for $\Sigma_i j(E)$ and Fig. 7, it is obvious that the TDF is vanishing when the band velocities are negligible. Importantly, the kernel K_2 is smaller than the kernel K_1. Thus the Seebeck coefficient as a function of the chemical potential is growing with the energetic range where the band extrema or termination occur. Summation over the band index in the TDF expression causes smoothing of the aforementioned features in the thermopower curve, which originate from the band manifod in comparison to those of the isolated bands. The most spectacular enhancements of the thermopower correspond to the energetic termination of the band manifold.

The effect is stronger for low temperatures but in a very tiny energetic range, which depends also on the band

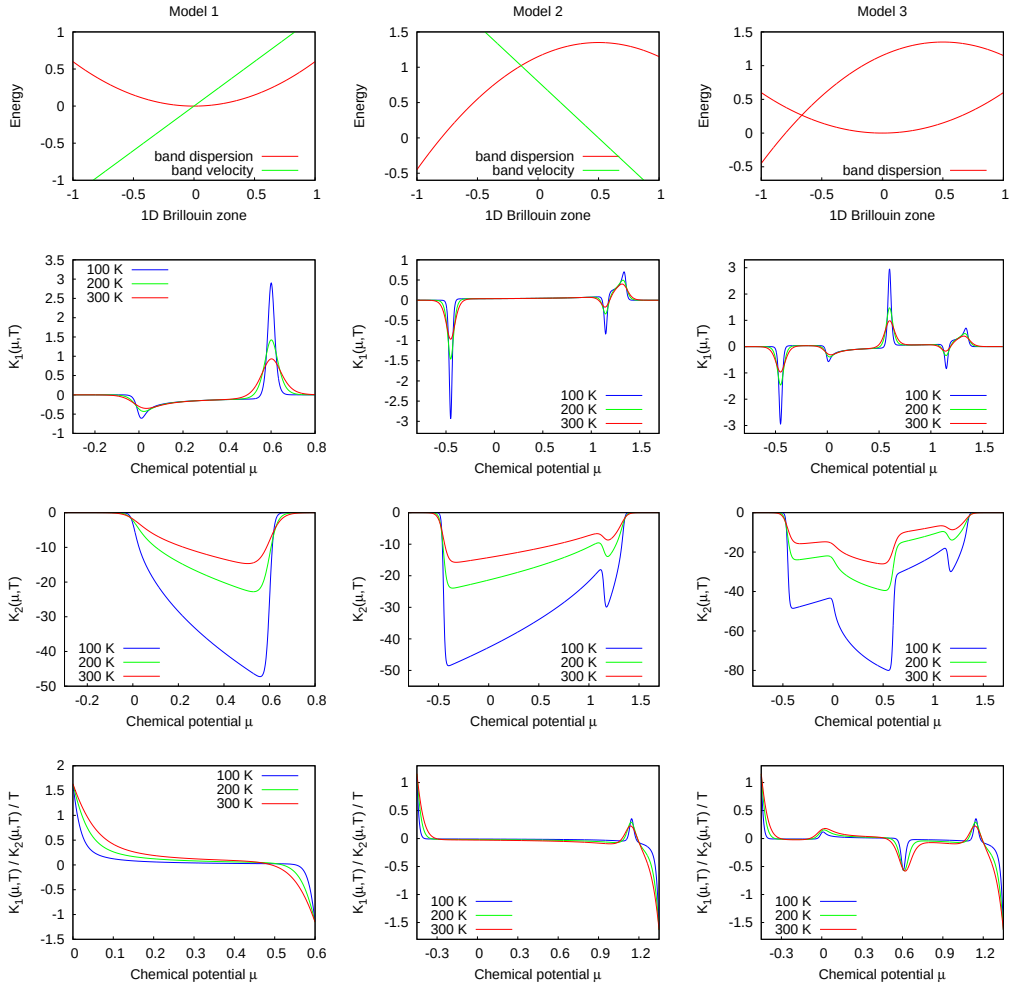

FIG. 7: Model band structures in 1D Brillouin zone and kernels of the expression for the Seebeck coefficient [in arbitrary units]. The constant relaxation time τ was assumed.

width of the given system. For higher temperatures, the thermopower growth is pronounced at wider energetic range and could be easier measured.

If we did not assume that the relaxation time was constant, the described features would be either better pronounced or smoothed depending on the τ dispersion. On the other hand, the band velocities do not change under the relaxation-time model. Thus, one can draw the conclusion that the band termination - within the energetic range - will enhance the thermopower in any case.

The phenomenon is general for many materials, especially for doped semiconductors where it should occur at the top of the valence band and the bottom of the conduction band. It applies also at the superconducting gap in the graphene-superconductor junction, as discussed by Wysokiński and Spałek in Ref. [38], and in the superconductor-ferromagnet junction in the presence of the magnetic field, as predicted by Ozaeta et al. in Ref. [39]. The same effect has been found recently in carbon nanowires by Tan et al. in Ref. [40], where large Seebeck effect showed up at the boundary of the zero-transmission windows. Interestingly, large growth of the thermopower should be observed in materials which have many flat bands, almost molecular-like states, such as molecular crystals or 2D organic semiconductors possess. In the perovskites, the flat band regions at Γ-X and X-M lines will certainly increase the thermopower, although these features are screened in the summation over the band index and **k**-space in the TDF expression. Similar effects have been observed in Ref. [41] for the electron doped $SrTiO_3$ and $KTaO_3$.

5. Conclusions

We investigated the thermoelectric properties of halfly H- and F-doped graphene. These systems are spin-polarized with the magnetic moments located at the undoped C-atoms. The effect of deposition on the C-face $4H$-SiC(0001) surface with two buffer layers have been also examined. The accurate calculations were performed for the band structures obtained from the density-functional theory and interpolated using the

maximally-localized Wannier functions, finally to be embedded in the Boltzmann equations. We found very interesting effect, which manifests with a huge growth of the thermopower and the ZT efficiency at the energies where the band manifolds terminate. The enhancement of the thermoelectric parameters at the band edges is a general property, not restricted to the graphene systems. This phenomenon deserves further investigations, in order to pave the way for two-digital values of ZT, and deny an inconvenient truth about the thermoelectrics that there are limitations for the search of efficient materials [9]. The interesting and technologically important fact is that the thermoelectric parameters at the band-termination energies can be very high at low temperatures, which is not plaussible in the ordinary high-ZT materials. Similar effects have been observed for gapped graphene [24], graphene-superconductor [38] and graphene-ferromagnet [39] junctions, and also graphene nanowires [40].

Acknowledgements

This work has been supported by the European Funds for Regional Development within the SICMAT Project (Contract No. UDA-POIG.01.03.01-14-155/09) and Operational Program Innovative Economy No. POIG.01.01.02-00-097/09 "TERMET - New structural materials with enhanced thermal conductivity". Calculations have been performed in the Interdisciplinary Centre of Mathematical and Computer Modeling (ICM) of the University of Warsaw within the grants G51-2 and G47-7, and by part supported by PL-Grid Infrastructure.

[1] Bauer GEW, Saitoh E, van Wees BJ. Spin caloritronics. Nature Mater 2012;11(5):391-399.
[2] Uchida K, Takahashi S, Harii K, Ieda J, Koshibae W, Ando K, Maekawa S, Saitoh E. Observation of the spin Seebeck effect. Nature 2008;455(7214):778-781.
[3] Uchida K, Xiao K, Adachi H, Ohe J, Takahashi S, Ieda J, Ota T, Kajiwara Y, Umezawa H, Kawai H, Bauer GEW, Maekawa S, Saitoh E. Spin Seebeck insulator. Nature Mater 2010;9(11):894-897.
[4] Uchida K, Adachi H, Ota T, Nakayama H, Maekawa S, Saitoh E. Observation of the longitudinal spin-Seebeck effect in magnetic insulators. Appl Phys Lett 2010;97(17):172505-4.
[5] Uchida K, Nonaka T, Ota T, Saitoh E. Longitudinal spin-Seebeck effect in sintered polycrystalline (Mn,Zn)Fe2O4. Appl Phys Lett 2010(26);97:262504-4.
[6] Jaworski CM, Yang J, Mack S, Awschalom DD, Heremans JP, Myers RC. Observation of the spin Seebeck effect in a ferromagnetic semiconductor. Nature Mater 2010;9(11):898-903.
[7] Sinova J. Spin Seebeck effect: Thinks globally but acts locally. Nature Mater 2010;9(11):880-881.
[8] Flipse J, Bakker FL, Slachter A, Dejene FK, van Wees BJ. Direct observation of the spin-dependent Peltier effect. Nature Nanotech 2012;7(3):166-168.
[9] Vining CB. An inconvenient truth about thermoelectrics. Nature Mater 2009;8(2):83-85.
[10] Tritt TM, Böttner H, Chen L. Thermoelectrics: Direct solar thermal energy conversion. Mater Res Soc Bull 2008;33(4):366-368.
[11] Verma R, Bhattacharya S, Mahapatra S. Thermoelectric performance of a single layer graphene sheet for energy harvesting. IEEE Transactions on Electron Devices 2013;60(6):2064-2070.
[12] Yin J, Zhou J, Li X, Chen Y, Tai G, Guo W. Enhanced gas-flow-induced voltage in graphene. J Appl Phys 2011;99(7):073103-3.
[13] Li X, Yin J, Zhou J, Wang Q, Guo W. Exceptional high Seebeck coefficient and gas-flow-induced voltage in multilayer graphene. Appl Phys Lett 2012;100(18):183108-4.
[14] Xing Y, Sun Q-F, Wang J. Nernst and Seebeck effects in a graphene nanoribbon. Phys Rev B 2009;80(23):235411-8.
[15] Liu T-H, Lee S-C, Pao C-W, Chang C-C. Anomalous thermal transport along the grain boundaries of bicrystalline graphene nanoribbons from atomistic simulations. http://dx.doi.org/10.1016/j.carbon.2014.03.005
[16] Nissimagoudar AS, Sankeshwar NS. Electronic thermal conductivity and thermopower of armchair graphene nanoribbons. Carbon 2013;52:201-208.
[17] Wei P, Bao W, Pu Y, Lau CN, Shi J. Anomalous thermoelectric transport of Dirac particles in graphene. Phys Rev Lett 2009;102(16):166808-4.
[18] Peres NMR, Lopes Dos Santos JMB, Stauber T. Phenomenological study of the electronic transport coefficients of graphene. Phys Rev B 2007;76(7):073412-4.
[19] Zeng M, Feng Y, Liang G. Graphene-based spin caloritronics. Nano Lett 2011;11(3):1369-1373.
[20] Zhao Y, Tang G-S, Yu Z-Z, Qi J-S. The effect of graphite oxide on the thermoelectric properties of polyaniline. Carbon 2012;50:2064-2073.
[21] Yazyev OV, Helm L. Defect-induced magnetism in graphene. Phys Rev B 2007;75(12):125408-5.
[22] Rudenko AN, Keil FJ, Katsnelson MI, Lichtenstein AI . Exchange interactions and frustrated magnetism in single-side hydrogenated and fluorinated graphene. Phys Rev B 2013;88(8):081405(R)-4.
[23] Park H, Wadehra A, Wilkins JW, Castro Neto AH. Spin-polarized electronic current induced by sublattice engineering of graphene sheets with boron/nitrogen. Phys Rev B 2013;87(8):085441-6.
[24] Sharapov SG, Varlamov AA. Anomalous growth of thermoelectric power in gapped graphene. Phys Rev B 2012;86(3):035430-5.
[25] Giannozzi P, Baroni S, Bonini N, Calandra M, Car R, Cavvazzoni C, et al., QUANTUM ESPRESSO: a modular and open-source software project for quantum simulations of materials. J Phys Condens Matter 2009;21(39):395502-19.
[26] Mostofi AA, Yates JR, Lee YS, Souza I, Vanderbilt D, Marzari N. wannier90: A tool for obtaining maximally-localised Wannier functions. Comput Phys Commun

2008;178(9):685-699.
[27] www.wannier.org
[28] Marzari N, Mostofi AA, Yates JR, Souza I, Vanderbilt D. Maximally localized Wannier functions: Theory and applications. Rev Mod Phys 2012;84(4):1419-1475.
[29] Pizzi G, Volja D, Kozinsky B, Fornari M, Marzari N. BoltzWann: A code for the evaluation of thermoelectric and electronic transport properties with a maximally-localized Wannier functions basis. Comp Phys Comm 2014;185(1):422-429.
[30] Borysiuk J, Bożek R, Grodecki K, Wysmołek A, Strupiński W, Stępniewski R, Baranowski JM. Transmission electron microscopy investigations of epitaxial graphene on C-terminated 4H-SiC. J Appl Phys 2010;108(1):013518-6.
[31] Haberer D, Petaccia L, Farjam M, Taioli S, Jafari SA, Nefedov A, Zhang W, L. Calliari, G. Scarduelli, B. Dora, D. V. Vyalikh, T. Pichler, Ch. Wöll, D. Alfé, Simonucci S, Dresselhaus MS, Knupfer M, Büchner B, Grüneis A. Direct observation of a dispersionless impurity band in hydrogenated graphene. Phys Rev B 2011;83(16):165433-6.
[32] Scheffler M, Haberer D, Petaccia L, Farjam M, Schlegel R, Baumann D, Hanke T, Grüneis A, Knupfer M, Hess C, Büchner B. Probing local hydrogen impurities in quasi-free-standing graphene. ACS Nano 2012;6(12):10590-10597.
[33] Zhu S, Li T. Hydrogenation-Assisted Graphene Origami and Its Application in Programmable Molecular Mass Uptake, Storage, and Release. ACS Nano DOI:10.1021/nn500025t
[34] Li C, Li G, Zhao H. Hydrogenation induced deformation mode and thermal conductivity variations in graphene sheets. Carbon 2014;72:185-191.
[35] Wierzbowska M, Dominiak A, Pizzi G. Effect of C-face 4H-SiC(0001) deposition on thermopower of single and multilayer graphene in AA, AB and ABC stacking. arXiv:1403.1286
[36] Strupiński W, Grodecki K, Wysmołek A, Stępniewski R, Szkopek T, Gaskell PE, Grüneis A, Haberer D, Bożek R, Krupka J, Baranowski JM. Graphene epitaxy by chemical vapor deposition on SiC. Nano Lett 2011;11(4):1786-1791.
[37] Wang XH, Yamamoto A, Eguchi K, Obara H, Yoshida T. Thermoelectric properties of SiC thick films deposited by thermal plasma physical vapor deposition. Sci Technol Adv Mater 2003;4(2):167-172.
[38] Wysokinski MM, Spałek J. Seebeck effect in the graphene-superconductor junction. J Appl Phys 2013;113(16):163905-5.
[39] Ozaeta A, Virtanen P, Bergeret FS, Heikkilä TT. Predicted very large thermoelectric effect in ferromagnet-superconductor junctions in the presence of a spin-splitting magnetic field. Phys Rev Lett 2014;112(5):057001-5.
[40] Tan XJ, Liu HJ, Wei J, Shi J, Tang XF, Uher C. Thermoelectric properties of small diameter carbon nanowires. Carbon 2013;53:286-291.
[41] Usui H, Shibata S, Kuroki K. Origin of coexisting large Seebeck coefficient and metallic conductivity in the electron doped SrTiO3 and KTaO3. Phys Rev B 2010;81(20):205121-6.